THE UNIVERSITY OF WARWICK

Interaction of large scale flow structures with gyrokinetic turbulence.

B.F. McMillan and P. Hill

Centre for Fusion, Space and Astrophysics, Department of Physics,

University of Warwick, CV4 7AL, Coventry UK

A. Bottino

Max Planck Institut für Plasmaphysik,

Boltzmannstr. 2, D-85748 Garching, Germany

S. Jolliet, T. Vernay, and L. Villard

Centre de Recherches en Physique des Plasmas,

Association Euratom-Confédération Suisse,

Ecole Polytechnique Fédérale de Lausanne, PPB, 1015 Lausanne, Switzerland.

(Dated: October 4, 2011)

Shear flows have a profound influence on turbulence-driven transport in tokamaks. The introduction of arbitrary initial flow profiles into the code ORB5 (Jolliet. et. al., Comp. Phys. Communications, **177**, 409) allows the convenient study of how flows on all length scales both influence transport levels, and self-consistently evolve. A formulation is presented which preserves the canonical structure of the background particle distribution when either toroidal or poloidal flows are introduced. Turbulence supression is possible above a certain shearing rate magnitude for homogeneous shear flows, and little evolution of the shearing rate is seen. However, when a flow with a zone boundary, where the shearing rate reverses at mid-radius, is introduced, the shear flow evolves substantially during the simulation. $E \times B$ shear flows with a zone boundary of a positive sign decay to a saturation amplitude, consistent with the well known saturation of turbulently generated zonal flows. Unlike the $E \times B$ flow, the parallel flows relax diffusively.

Gyrokinetic turbulence modelling indicates that the self-consistent flows driven by drift wave turbulence can substantially suppress transport levels in tokamaks. Imposing a ho-

mogeneous background (toroidal or poloidal) flow shear can reduce transport levels even further. However, the physics of turbulence-scale and global-scale flows have been investigated as separate topics. A comprehensive understanding of the physics of the interaction between shear flows on the full range of length scales and turbulence is lacking.

For example, the process which limits the amplitude of self-consistently driven shear flows has not been seen to act on homogeneous flow shears applied as an initial condition. We would like to know what supresses this saturation mechanism for large-scale flows. Understanding this is particularly crucial for the physics of transport barriers, where flow structures form on intermediate length scales.

We study this problem numerically using the global gyrokinetic code ORB5[1]. In order to systematically investigate both homogeneous shear flows, and the zig-zag type flows seen in quasi-steady state gyrokinetic simulations, we allow arbitrary flow profiles as an initial condition in the code. This requires a definition of the background gyrocentre distribution f_0 which allows poloidal and toroidal flows with arbitrary profile. In order that f_0 remains a canonical distrubution (*i.e.*, constant along trajectories when the perturbed electric field is zero), the background electrical potential enters into the definition of the distribution function.

We then perform a series of numerical tests to examine how the structure of the background shear flow modifies turbulence levels, and to examine the dynamics of the flow structures. First, the effect of a homogeneously sheared background flow is examined, partly as a benchmark against previous simulations. Secondly, we examine the linear and nonlinear evolution for 'V-shaped' flow profiles where the sign of the flow shearing rate changes at mid radius. The *zone boundaries*, where the sign of the flow shearing rate changes, are shown to play a critical role in self-consistently limiting the shearing-rate.

I. GLOBAL GYROKINETIC EQUILIBRIA WITH BACKGROUND SHEAR FLOW

We consider small background flows, with $v_e/v_{th} \ll 1$, so that we ignore the transonic terms that arise when the $E \times B$ flows are of order 1. Note however, that we expect to largely recover the effects of the Coriolis and centrifugal forces for toroidally rotating plasmas, which are mostly associated with strong flow along the magnetic field[2]. In this limit the standard

gyrokinetic formulism is valid, and we simply start from a different initial condition for the flow and electric field. To consider plasmas with a background electric potential ϕ_0, we consistently modify the background distribution f_0, and substitute $\phi \rightarrow \phi_0 + \phi$ in the zeroth order gyrokinetic equations of motion. We also introduce parallel flows in f_0 such that the sum of the $E \times B$ and parallel flows is either dominantly poloidal, or dominantly toroidal. The Vlasov-Poisson equations are unmodified, but the equations for δf are modified due to the different f_0. In principle we could add an initial flow in the initial perturbation δf_0, but incorporating the flow perturbation in f_0 means that $\delta f / f$ and therefore noise can be reduced, and linear dynamics can be conveniently treated.

Here, we require that the background distribution function be a collisionless gyrokinetic equilibrium, so that f_0 is constant along the unperturbed gyrocentre orbits. If the background equilibrium is chosen to be a local Maxwellian, as in some gyrokinetic codes, one must either tolerate large transient fluxes at the beginning of the simulation, or ignore terms arising from the derivatives of f_0 along the gyrocentre trajectory.

In order for f_0 to be a collisionless equilibrium, f_0 must only be a function of the three canonical momenta: the energy $\epsilon = mv^2/2 + q\phi_0$, toroidal canonical momentum $\psi_c = \psi(\vec{R}) + mv_\parallel RB_\zeta / qB$ and magnetic moment μ. We supress the gyroaveraging for the background field ϕ_0, which will vary on scales considerably longer than the gyroradius. We define a canonical Maxwellian

$$f_0 = \frac{n_0(\Upsilon)}{(2\pi T(\Upsilon)/m)^{3/2}} \exp\left(-\frac{\epsilon - q\phi_0(\psi_*)}{T(\Upsilon)}\right), \tag{1}$$

where $\psi_*(\psi_c, \epsilon, \mu)$ is a modified canonical momentum which will be chosen later, and Υ is the 'corrected' canonical momentum defined in ref. [3]. The toroidal canonical momentum is equal to the poloidal flux at zeroeth order in $\rho*$, and thus can be used as a radial parameter; in the $\rho* \rightarrow 0$ limit, this equilibria is locally Maxwellian, with temperature and density varying as a function of radius. To make the dependence on ϕ_0 more explicit, the exponent in the definition of f_0 can be written $[mv^2/2 + q\phi_0(\psi) - q\phi_0(\psi_*)]/T$. The addition of the $q\phi_0(\psi_*)$ term is necessary in order that $\int dv^3 f_0 \sim n_0$, so that the density and the electric potential can be independently specified.

The initial electron density is assumed to almost neutralise the initial ion density, to give the prescribed initial electric field. In practice, we do not calculate the n_e exactly, but instead, the approximation $n_e(\psi) \sim n_0(\psi) \sim< f_0 >$ is used for the electron density which

appears in the quasineutrality approximation, neglecting terms of order $\rho*$.

The equations of motion are as before, except with an $E \times B$ flow incorporated into the equations of motion:

$$\frac{dR}{dt} = \frac{v_\parallel}{B*_\parallel}\vec{B*} + \frac{v_\perp^2}{2\Omega_i BB*_\parallel}\vec{B} \times \nabla B + \frac{\left(E_0 + <\vec{E}_1>\right) \times \vec{B}}{BB*_\parallel} \quad (2)$$

and

$$\frac{dv_\parallel}{dt} = \frac{\vec{B*}}{m_i B*_\parallel} \cdot \left(\frac{m_i v_\perp^2}{2B}\nabla B + q_i \nabla\left(\phi_0 + <\phi_1>\right)\right) \quad (3)$$

The evolution equation for $\delta f = f(R,t) - f(R,t_0)$ is then:

$$\frac{d\delta f}{dt} = -f_0\kappa(\Upsilon)\frac{d\Upsilon}{dt} + \frac{q_i f_0}{T_i(\Upsilon)}<\vec{E}> \cdot \left.\frac{d\vec{R}}{dt}\right|_0 - \frac{f_0 q}{T_i(\Upsilon)}\frac{d\phi_0(\psi_*)}{d\psi_*}\frac{d\psi_*}{dt}, \quad (4)$$

with

$$\kappa(\Upsilon) = \frac{n_0'(\Upsilon)}{n_0'(\Upsilon)} - \frac{3T_i'(\Upsilon)}{2T_i(\Upsilon)} + \frac{[\epsilon - q\phi_0(\psi_*)]T_i'(\Upsilon)}{T_i(\Upsilon)^2} \quad (5)$$

The $f_0\kappa d\Upsilon/dt$ term arises as before from the density and temperature gradients, and the second term results from the modification to the gyroenergy as the particles interact with the perturbed electric field. The third term arises directly from the inclusion of ϕ_0 in the definition of f_0. Note that all three terms are modified due to the modified marker trajectories.

Choosing $\psi_* = \psi_c$, the canonical toroidal momentum, results in the a near 'pure toroidal flow' case, with small poloidal flows arising from temperature and density gradients. The poloidal component of the parallel flow along the field line cancels the poloidal flow due to the $E_0 \times B$ motion. Parallel flow appears because $\psi - \psi_c$ is proportional to the parallel velocity, and $\phi_0(\psi_c) - \phi_0(\psi) \propto E_r v_\parallel$: the distribution (ignoring for a moment the density and temperature gradients) is simply a shifted Maxwellian in the small E_r limit. Because collisions are thought to keep the distribution quite close to neoclassical equilibrium for most fusion relevant parameters, it is desirable that our background equilibrium be close to neoclassical equilibrium. For $\psi_* = \psi_c$ the solution is an exact neoclassical equilibrium for the case where there is zero temperature gradient and $\partial\phi_0/\partial\psi$ constant (with only ion-ion collisions); once temperature gradient is introduced, the departure from neoclassical equilibrium is small, of order ρ^*.

On the other hand, choosing

$$\psi_* = \psi_{c'} = \psi(\vec{R}) + Fv_\parallel/B - F<v_\parallel/B>, \quad (6)$$

which we call the modified canonical toroidal momentum, results in a state with small parallel flows. Here, the angle brackets denote a bounce average along zeroth order trajectories. $\psi_{c'}$ is equal to the bounce average of ψ, so that is can be considered a good 'average radial position' variable. This choice minimises the distortion to the distribution function f_0 due to ψ_0, by reducing the RMS magnitude of the term $\psi_0(\phi) - \psi_0(\psi_c')$. However, once the electrical potential difference across a banana orbit $qE_r\rho_i(a/Rq)^{1/2}$ becomes comparable to the thermal energy, f_0 departs strongly from Maxwellian: collisionless equilibria with poloidal flows are inherently far from local Maxwellian. For large enough flows, the distribution function becomes double-peaked, due to structures at the trapped-passing boundary, and may well be unstable to bump-on-tail instabilities (which would not be correctly modelled in the gyrokinetic ordering and on the spatial scales resolved). In practice, with $q \sim 2$ and $R/a \sim 3$, this leads to a restriction to poloidal flows $\lesssim 0.1v_{th}$, because we have assumed that the distribution function is near-Maxwellian in our derivation of the gyrokinetic equations, and simulations with larger flows manifest flow-driven instabilities which we would not expect to correctly resolve. It is interesting that there may be a mechanism limiting the size of poloidal flows even in strictly collisionless toroidal devices.

Plasma flows driven by the flux-surface averaged component of the electrical potential are capable of secularly tilting turbulent structures superimposed on the flow. The main impact of these sheared flows can be captured by an effective shearing rate,

$$\omega_{E\times B} = \frac{r}{qB}\frac{d}{dr}\left(\frac{q}{r}\frac{d\phi_0}{dr}\right) \tag{7}$$

which gives the rate at which turbulent structures will be sheared in the poloidal plane, once an overall toroidal propagation has been factored out.

To substantially stabilise drift wave turbulence with shear flows, the effective shearing rate would have to be similar to typical growth rates. For a homogeneous flow shear with effective shearing rate of the order of (for example) the typical ITG growth rate $0.1c_s/a$, over the whole minor radius, we would have $E \times B$ shear flows $\sim 0.1v_{th}$ at the plasma edge. Poloidal flows of this size would usually violate the assumption that f_0 be close to Maxwellian. Toroidal flows would need to be $\sim v_{th}$, for typical $q \sim 2$ and $R/a \sim 3$, too large to be correctly modelled without adding transonic terms into our gyrokinetic model, and much larger than seen in typical measurements in the cores of tokamaks. For standard parameter choices, it is only possible to introduce large enough flow shear to substantially

modify the turbulence, within the limits of our ordering, by restricting the region with strong shear flow to an interval of the minor radius: for example, in a localised internal transport barrier.

The local density and mean kinetic energy are not substantially modified by the imposition of a background electric field, for moderate values of the electric field strength, so that the specified $T(r)$ and $n(r)$ are very close to the reconstructed initial $T(r, \theta)$ and $n(r, \theta)$ found by taking moments (which would trivially be the case in codes which use a local Maxwellian as an initial condition). This is important in order to conveniently specify the initial profiles in a simulation. Also, we have implicitly assumed that the electron density and background potential are flux surface functions, which would be inconsistent if the ion density varied with poloidal angle.

II. SIMULATIONS WITH UNIFORM SHEAR FLOWS

A series of simulation scans with two different plasma configurations were performed, with homogeneously sheared toroidal and poloidal flows. The STD case used in ref. [4], which also investigated stabilisation with shear flow, serves as a convenient choice for benchmarking. For this case, $q = 2$, $(r/q)dq/dr = 1.0$, $R/L_T = 9$ at midradius, and $a/R = 1/3$. The Cyclone case, which has been used in many other investigations, is also an obvious choice as a baseline; we choose a slightly higher temperature gradient, however, because we are interested in situations where flow shear stabilisation leads to substantially improved confinement. For this Cyclone-like case, $q = 1.4$, $(r/q)dq/dr = 0.8$, $R/L_T = 8$ at $r/a = 0.5$, and $a/R = 0.36$. Circular concentric model equilibria are used for both simulations. The simulations were run using an adiabatic electron model. In order to limit the flow amplitude at the inner and outer simulation boundaries, while treating a reasonably broad turbulent region, $> 100\rho_i$, the simulations were run at fairly small $\rho^* = 1/400$, on an annular domain $r \in [0.3, 0.83]$. Noise was controlled using a Krook operator with damping rate $0.008c_s/a$, as desribed in Ref. [5], but with toroidal flow conservation also enforced.

First, a set of linear simulations were run for the Cyclone case, with pure poloidal flows, and it was found that a background flow with a shearing rate of $0.05c_s/a$ is sufficient to almost completely stabilise the system (fig. 1), although there is a small residual growth rate of $\sim 0.009c_s/a$. Strong linear supression with arbitrarily small values of flow shear would

be predicted in flux tube simulations[6], because adding a small flow qualitatively changes the nature of the linear spectrum, in much the same way as adding a small resistivity fundamentally changes the nature of the ideal MHD spectrum. We find a somewhat less dramatic, but still strong, stabilisation in this global analysis. Interestingly, the maximum growthrate in these simulations occurs not for zero flow shear, but for small positive flow shear: the profile shearing which results from the radial variation of the local mode frequency $\omega(r)$ is exactly cancelled by the flow shear at this point. Secondly, a nonlinear scan of Cylone cases were run with shearing rates $[0, \pm 0.025, \pm 0.05, \pm 0.10, \pm 0.12, \pm 0.15, \pm 0.2](a/c_s)$. It was necessary to start nonlinear simulations with large initial perturbations, as in ref. [4], because the cases with large shear are marginally or completely linearly stable, and the simulations are run over a relatively short timescale of $[0, 800]a/c_S$. Substantial heat fluxes are seen for shearing rates several times larger than the point where linear growth rates are almost zero, so that there is a broad region of subcritical turbulence. The nonlinear stabilisation by the sheared flow therefore cannot be directly explained by a reduction in linear growthrates: quasilinear predictions would be expected to be problematic in plasmas with shear flow.

The changes in radially averaged shearing rate during the simulations, which fall in the range $[-0.02, 0.03](c_s/a)$, are much smaller than the range of shearing rates considered, $[-0.2, 0.2]$, so the conclusions on the effects of shearing rate remain the same whether we use the initial or final shearing rates for comparisons. Fig. 1 shows the thermal diffusivities in the simulation versus the shearing rate. Despite some scatter, the dependence of thermal diffusivity on shearing rate can be well modelled by parabolas except for the highest shearing rates where turbulence is supressed entirely. The turbulence is entirely supressed when the shearing rate is $|\omega_s| \sim 0.8\gamma_{ITG}$ or $\sim 1.0\gamma_{ITG}$ for poloidal and toroidal flows respectively. Ref. [4] also saw evidence of subcriticality for initial shearing rates close to the quench point, where large perturbations were required to acheive sustained turbulence: this phenomenon is more marked in our Cyclone simulations, which required large initial perturbations even for relatively small shearing rates, $\omega_s \geq 0.05c_s/a$. For the simulations with substantial thermal diffusivity and toroidal flows, the flux of parallel momentum $\Gamma_\parallel$ is roughly proportional to the product of the radial derivative of the parallel flow profile and the heat flux. The ratio of the effective momentum diffusivity to the heat diffusivity, the Prandtl number, found by linear fitting, is ~ 0.4.

We also ran simulations with relatively large shear-free rotation of $0.04c_s$ and $-0.04c_s$, and found a diffusivity of 2.6 and $2.5\chi_{GB}$ respectively, indicating that diffusivity is largely independent of the flow rate over the range $[-0.04, 0.04]c_s$. The maximum flow rate $v_{E\times B}$ in the sheared simulations is $0.04c_s$. We therefore do not expect the magnitude of the flow to influence the diffusivity in the inner and outer parts of the sheared simulations.

For the STD case, a scan was conducted for shearing rates over the range $[-0.145, 0.145]c_s/a$ with pure toroidal flows, and $[-0.09, 0.09]c_s/a$ with pure poloidal flows. The diffusivities agree relatively well with the adiabatic electron cases in ref. [4] and ref. [7], for either sign of shearing rate; the local simulations are expected to be insensitive to the sign of the shearing rate for up-down symmetric equilibria, due to a symmetry of the local gyrokinetic equations. Although we do not plot it here, the uncertainty due to turbulent fluctuation is of the order of 20%. The range of shearing rates examined here is somewhat smaller than those in refs. [4] and [7] in order to avoid excessively large flows near the inboard and outboard edge of the annulus: to examine larger shearing rates we would need to consider a smaller annulus of a larger plasma, nearer the local limit. The Prandtl number, is around 0.5 (for the three cases with nonzero velocity shear), in rough agreement with [7], although the scatter is too large to recover the dependence on shear.

Notably, both poloidal and toroidal shear flow allow complete turbulence stabilisation in the Cyclone case, whereas in the STD case, toroidal shear flow does not substantially suppress turbulence. In the Cyclone case, the toroidal shear flow required to produce a substantial shear on the turbulent structures is considerably lower (due to lower q and R/a), and the temperature gradient is relatively close to critical. This may explain why the destabilising effects of parallel shear flow which is introduced when considering toroidal, rather than poloidal, shear flows, is weaker in the Cyclone case.

Figures 3(a), and 3(b) show inward propagating bursts across the simulation domain for positive shearing rates and outwards propagating bursts for positive shearing rates. This can be quantitatively confirmed by considering 2D autocorrelation diagrams, as in ref. [8]; the dominant correlations along the lines $\delta r = v\delta t$, where v is the burst velocity, suggest that most of the time variation in heat flux is associated with bursts. This is consistent with the results and theory presented in ref. [8]. We also observe a shift in the diffusivity profile as a function of shearing rate (Fig. 2), which may be due to a process which we call 'turbulence convection' in analogy with the 'turbulence spreading' proposed by others[9]: the
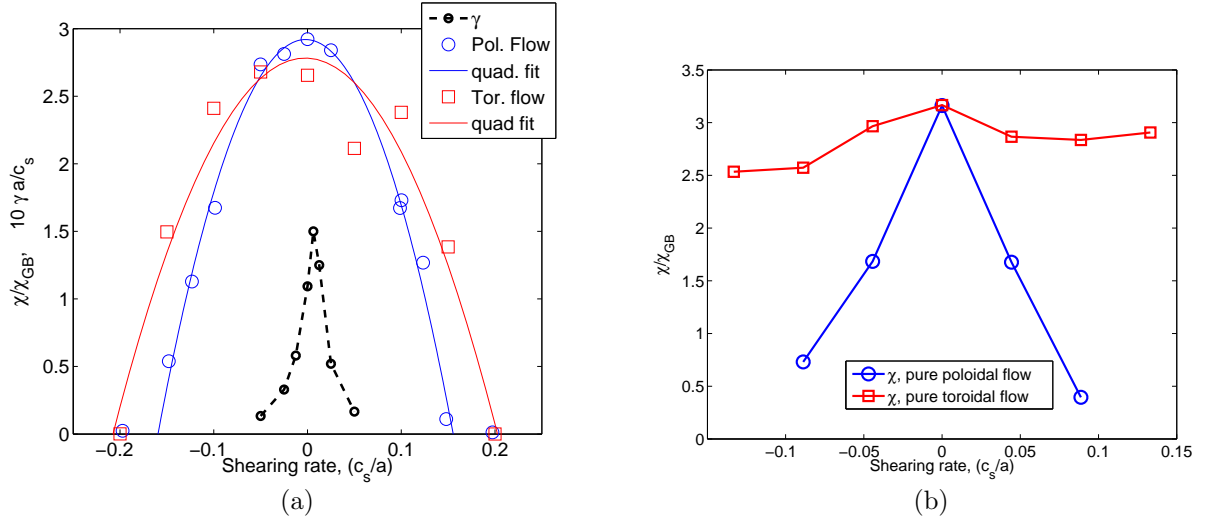
FIG. 1: Diffusivity versus shearing rate for pure poloidal flow (large circles), and for pure toroidal flows (squares), for the (a) Cyclone case and (b) Waltz standard case. In the left subplot, quadratic fits of these points are shown (solid lines, extreme cases with complete stabilisation have been omitted from the fit), with maximum ITG growth rate for these cases shown as a dashed line (small circles). (colour online)

bursts carry information about turbulence levels across the minor radius, which may modify the steady state fluxes that would be expected in a local picture. Given that bursts can propagate across a large proportion of the turbulent region, simulation results in the centre of the annulus may depend on boundary conditions, because the bursts could be generated at the boundary. This is despite the active region being 150 gyroradii wide, comparable to the radial extents used in typical flux tube calculations, and a sizeable proportion of the width of the core in experiments like JET.

III. SIMULATIONS CONTAINING ZONE BOUNDARIES

Quasi-steady state turbulently generated flows tend to self-organise into a zig-zag structure, with alternating domains of roughly constant positive and negative poloidal flow shear. To model a plasma contaning a boundary between two flow zones, we consider a 'V-shaped' flow profile, with two zones of opposite but equal flow shear, and set the interface between the two zones at roughly mid-radius, as shown in figure 4. Here we have flow shear profiles
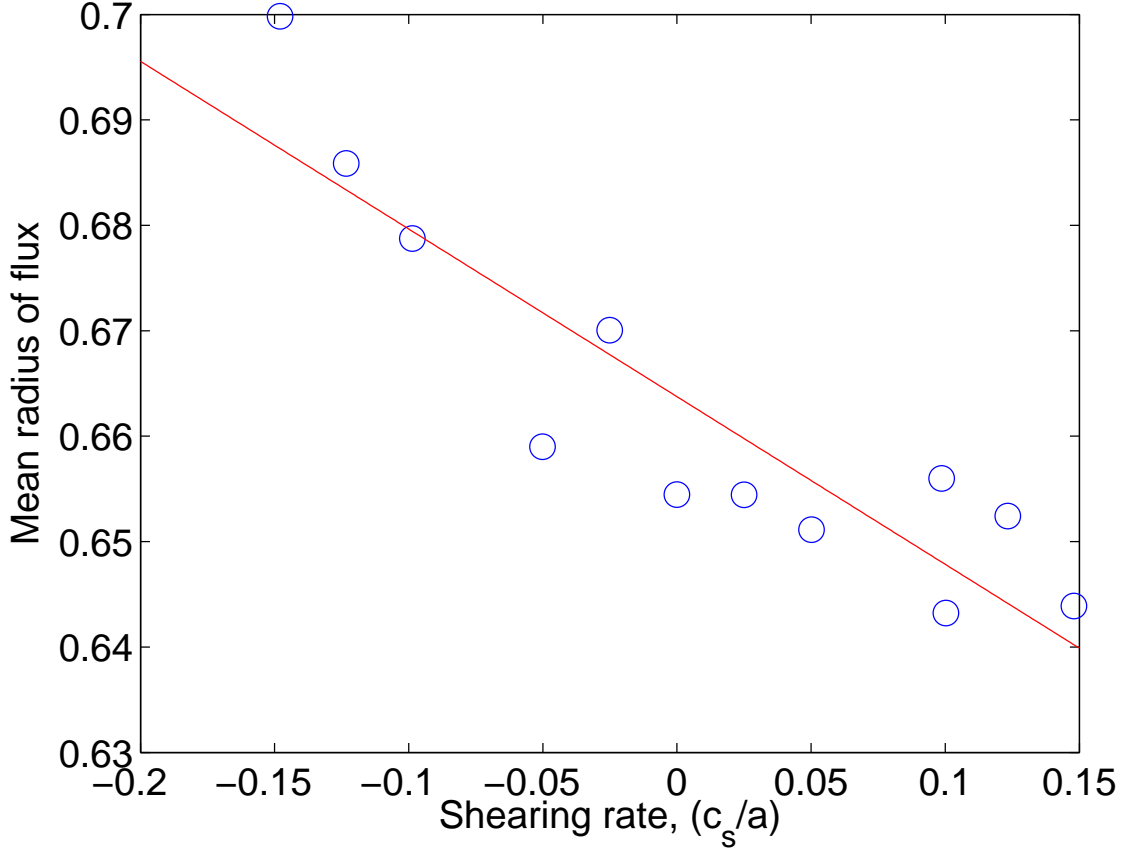
FIG. 2: The mean position of the heat flux profile, $< r\Lambda > / < \Lambda >$, as a function of shearing rate. A linear fit is show for comparison.

of the form

$$\omega(r)_{E \times B} = -\omega_v \text{sign}(r - r_0). \tag{8}$$

First, we perform a linear stability analysis of the Cyclone test case with poloidal 'V-shaped' flows of varying amplitude, ω_v, and at different values of temperature gradient. In linear simulations with V-shaped flow, the unstable mode is radially localised near the zone boundary; the strong linear stabilisation resulting from homogeneous flow shear appears to be enough to locally damp the mode away from this inhomogeneity. At low values of temperature gradient (fig. 5) introducing flow shear reduces the growth rate. Note that the stabilisation with flow shear depends strongly on the sign of the 'V', and that positive V-flows are much less effective for stabilisation. For large enough negative V-profiles, and larger temperature gradients, the plasma becomes more unstable with increasing shear, so that only a finite 'window' in flow shear is stable. At a certain temperature gradient ~ 6.3, there is no longer
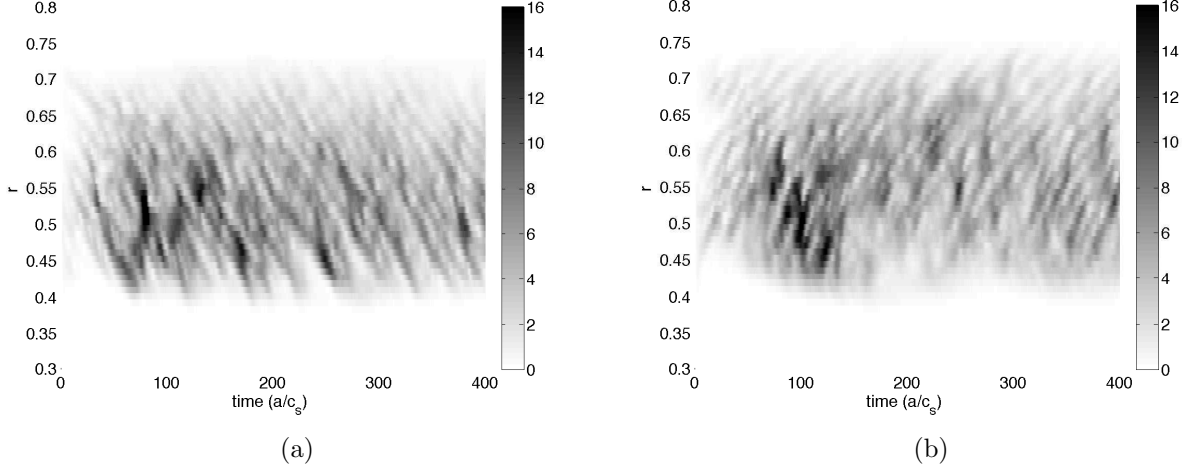
FIG. 3: Flux versus time and radius for the Cyclone-like simulations with background shear (a) $0.1a/c_s$ and (b) $-0.1a/c_s$.

any stable value of ω_v. This should be contrasted with the situation for homogeneous shear flows (see fig. 1(a)), where a shearing rate of $0.05c_s/a$ is sufficient to almost completely stabilise the flows at $R/L_T = 8.3$, higher than any considered here.
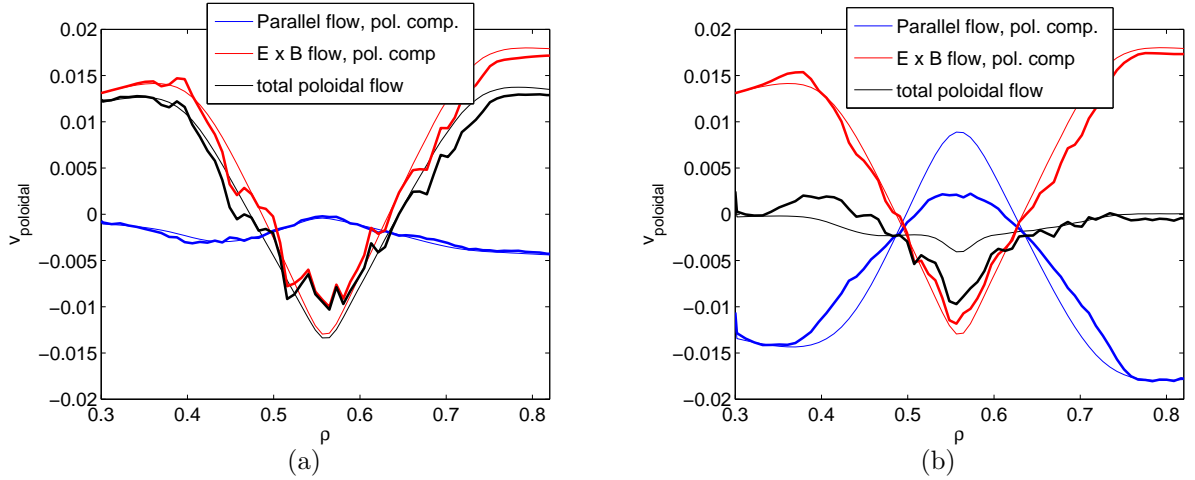

FIG. 4: Components of poloidal flow for simulations with an imposed V-shaped poloidal flow (a) and toriodal flow (b) with $\omega_v = 0.2$. The initial profiles, and those at the end of the simulation are shown as thin lines, and thick lines, respectively (colour online).

As a rough method to characterise the interaction of these linear modes with the poloidal flow, we consider the profiles of radial gyrocentre flux Γ. This gyroflux induces a prompt modification of the axisymmetric radial electric field. The zonal electric field is also influenced by a radial redistribution which occurs on the bounce time due to the parallel velocity

dependence of the perturbation[10], which we do not analyse. In figure 6 we plot Γ normalised to the maximum heat flux for the linear eigenmodes of the $R/L_T = 6.94$ case. In each case the gyrodensity perturbation produced by the flux would act to reduce the flow at the zone boundary. By far the strongest normalised gyrocentre flux occurs for the case with large positive V-profile.

The fact that there are stable equilibria with flow above the zero-flow stability limit can be considered a manifestation of the Dimits shift. The temperature gradient where all flow states are unstable (between $R/L_t = 6.25$ and 6.94) is roughly equal to the nonlinear critical gradient in Ref. [11]. An analogous linear stability analysis was performed in Ref. [12] for a sinusoidal flow profile, to determine the range of existence of such states.
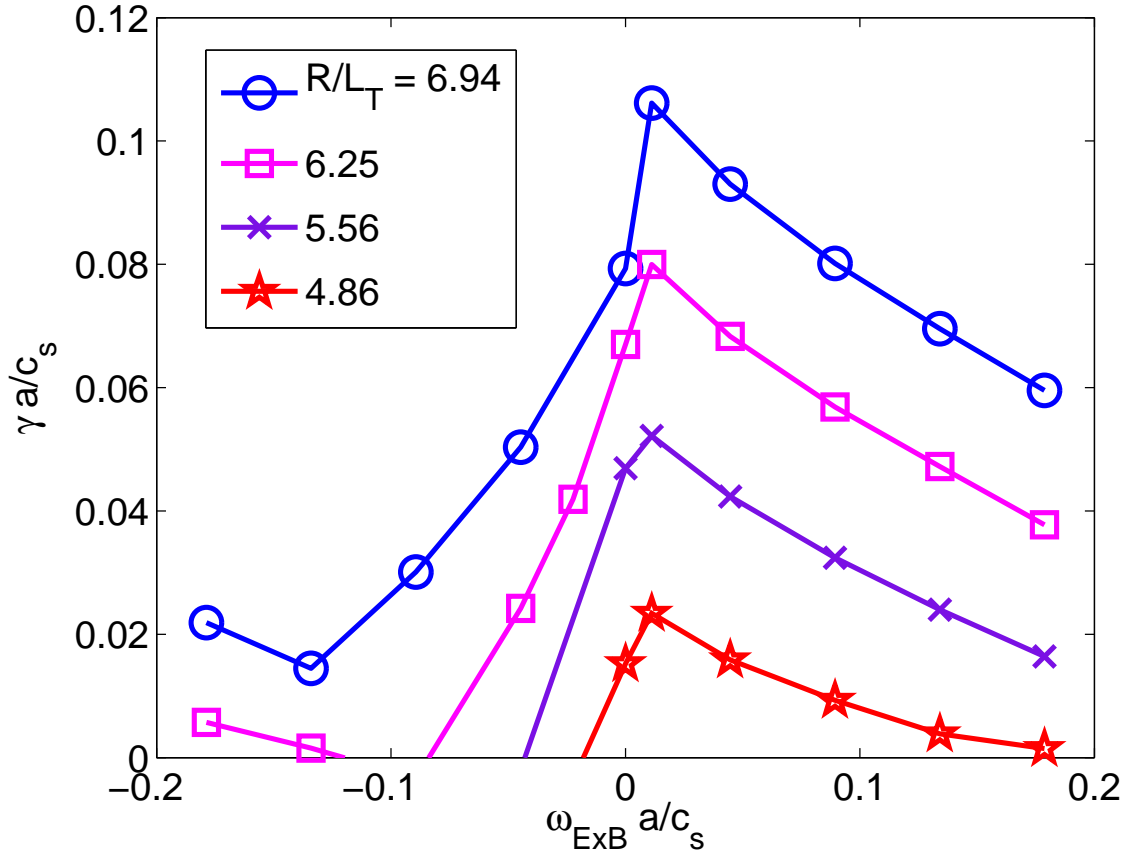

FIG. 5: ITG growth rate versus imposed flow shear amplitude for 'V-shaped' flow profile. (colour online)

A nonlinear scan is then performed to further investigate shear flow supression, with V shaped flows, at $R/L_{T0} = 8.0$. In these simulations, in contrast to the simulations with
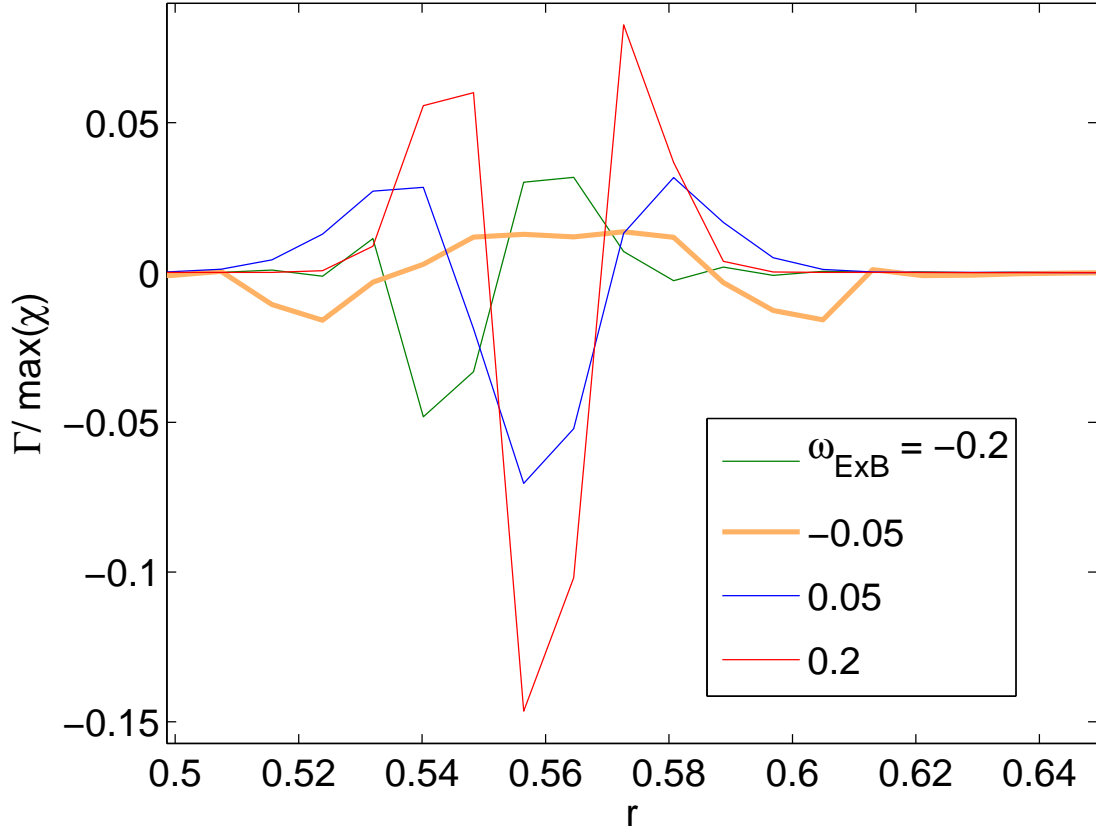
FIG. 6: Gyrocentre flux versus radius, normalised to maximum heat flux, for V-shaped profiles, with $R/L_T = 6.94$. (colour online)

homogeneous shear, the overall flow profile undergoes substantial time evolution when the initial V shaped flow is strongly positive: the turbulently generated flows act to reduce the peak flow in this case. To quantify this reduction in global shear, we measure the overall $E \times B$ shearing rate in the left (ω_l) and right (ω_r) half of the 'V', and define an large-scale shearing rate ω_{ExB}^* as $\omega_l/2 - \omega_r/2$. At the start of the simulation, $|\omega_{ExB}^*|$ is equal to the mean absolute value of the shearing rate. We plot the diffusivity versus initial and final ω_{ExB}^* in fig. 7(a). Unlike in the simulations of the previous section, there is a marked tendency for the ω_{ExB}^* to decrease. For large enough initial V-shaped flow, the final ω_{ExB}^* decreases to roughly $0.12c_s/a$, indicating that there is a saturation mechanism acting to limit the global shear. For these cases, ω_{ExB}^* stabilises an its final value about $300a/c_s$ into the nonlinear period. Even for $\omega_{ExB}^* < 0.12c_s/a$, the value of ω_{ExB}^* decreases somewhat during the simulation, so that for negative V-flows, the absolute shear actually increases. It is well

known from previous gyrokinetic simulations that small-scale zonal flow shear to saturate at $\sim 0.2c_s/a$: this also occurs for positive V-shaped flows on long length scales.

The late time diffusivity is not strongly dependent on the sign of the flow profile, but only the magnitude of the late time ω^*_{ExB}. The average late time heat flux both in these simulations and those of the previous section is well predicted by the late time $|\omega^*_{ExB}|$ (the parabolic fit used in 1 is reproduced in 7 for comparison). However, this is no longer the case when the early time behaviour is considered. The simulations with large initial positive V-flow, show large diffusivity in the early stages, $2-3\chi_{GB}$, as the flow profile evolves towards saturation, unlike the simulations with large negative V-flows, which show almost complete turbulence supression. To accurately quantify the diffusivity levels for large positive V-flows, we would need to artificially maintain the global flow profile: nevertheless, we conclude that positive V-flows are less effective for turbulence supression than negative V-flows.

The complete supression of late-time turbulence seen at the largest negative ω_v is not surprising given the very strong (but not complete) linear stabilisation at $R/L_T = 6.94$. At positive ω_v, the linear theory suggests only a small supression of turbulence at the zone-boundary. This is broadly consistent with the high levels of turbulence seen in the nonlinear simulations with large positive ω_v at early time. Unlike in the case with homogenous shear flows, the regimes of linear and nonlinear stability coincide moderately well. The much stronger flow profile evolution seen for cases with large positive ω_v is also consistent with the large normalised gyrodensity flux in linear modes at large positive ω_v (assuming that ratio between heat flux and gyrodensity flux stays roughly constant in the nonlinear regime).

The stronger linear stability, and lower diffusivity for negative ω_v provides a plausible explanation for the correlation between E_r and the perturbed temperature gradient $\delta(R/L_T)$ seen in earlier ITG simulations[13, 14]. Figure 8 shows the temperature gradient fluctuation and E_r profile averaged over $60a/c_s$ in an earlier CYCLONE-type simulation with $\rho^* = 1/280$, and no heat source. We can clearly see that the temperature gradient profile and the E_r profile are correlated on short scales but not exactly proportional: the strong change in temperature gradient at the edge of the turbulent region is not really reflected in E_r. Radial profiles of temperature gradient and E_r show corrugations on the zonal flow wavelength, with lower R/L_T at negative zone boundaries, and higher R/L_T at positive zone boundaries; lower temperature gradient compensates for the larger diffusivity in order that the heat flux be radially uniform.
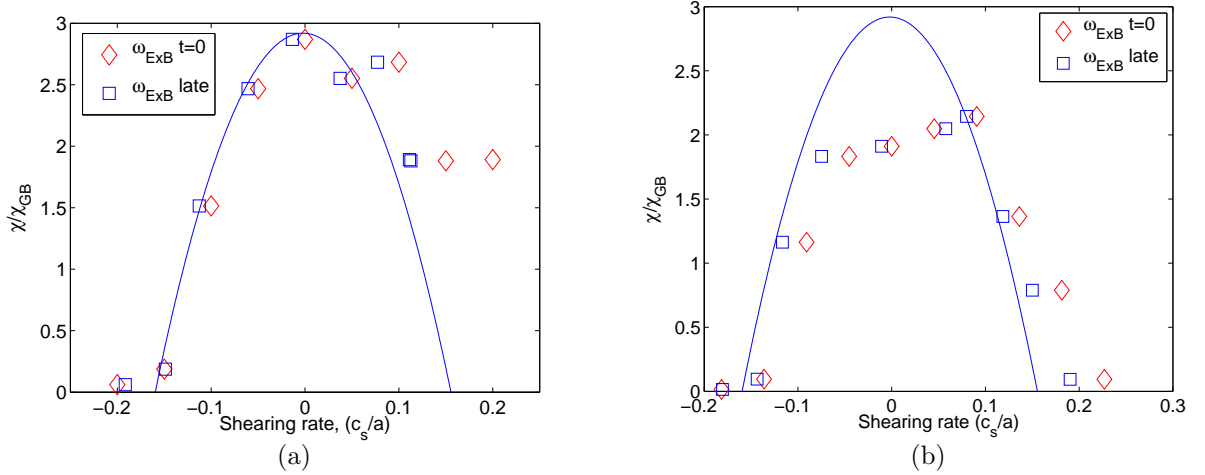
FIG. 7: Diffusivity versus large-scale shearing rate, ω^*_{ExB}, for simulations with an imposed V-shaped poloidal flow (a) and toriodal flow (b). Diamonds show initial ω^*_{ExB} and squares show ω^*_{ExB} averaged over the last half of the simulation. The parabola is the fit from 1, where a homogeneous flow was imposed. (colour online)

Other authors have suggested that the sum of the diamagnetic and $E \times B$ flow is dynamically conserved even in collisionless simulations[13], or found similar correlations during bursts in weakly collisional simulations and ascribed them to radial force balance[14]. However, it is clear from figure 8 that the sum of the diamagnetic ($\propto dT/dr$) and $E \times B$ flows is not conserved, and we know of no reason to expect this quantity to be conserved except on the collision timescale.

An important difference between the physics with positive and negative V-shaped flow is the propagation of bursts in the system. Again, the burst direction depends on the local sign of the flow shear, so bursts travel outwards from (inwards towards) the zone boundary for positive (negative) V-flows. Dynamics at the positive V-boundary might therefore be expected to have a strong nonlocal effect on the plasma.

When V-shaped toroidal flows are specified, the overall dynamics are similar to the simulations with V-shaped poloidal flows. The E_r profile evolution is similar, as is the thermal transport level. We were able to perform a wider scan in initial shearing rate with pure toroidal flows than poloidal flows, because the restriction that the toroidal flow be a small fraction of the sound speed is less strict that the requirement for poloidal flows not to excessively distort the background distribution. One complication that arises when V-shaped
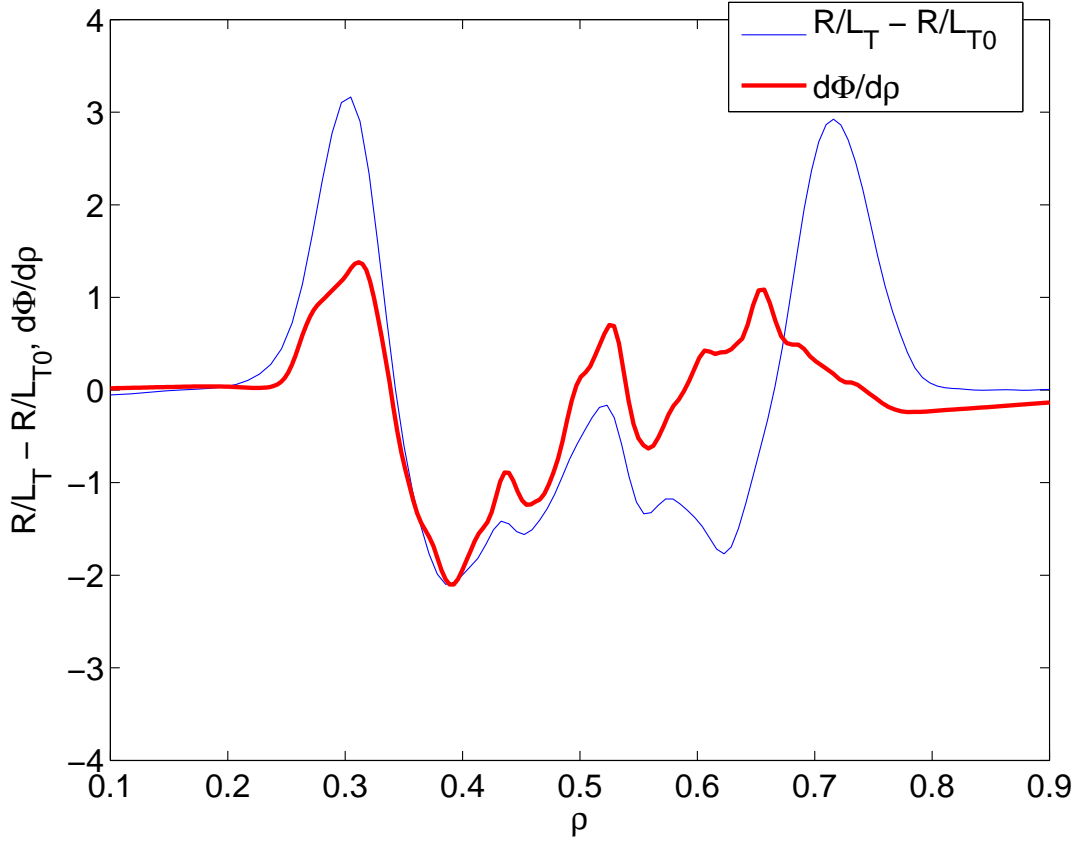
FIG. 8: Profiles of temperature gradient fluctuations (thin line) and the radial derivative of the zonal potential (thick line) versus radius, averaged over the last $60a/c_s$ of an ITG simulation without a heat source. (colour online)

toroidal flows are added is that the reconstructed temperature gradient profile becomes somewhat sensitive to the input parameter ω_v, with a bump or hole appearing at the reversal point (this effect is proportional to ρ^*). For these simulations, we turn off the heat source inside the turbulent region $[0.4, 0.7]$, to allow the temperature profile to relax to a self-consistent steady state: the localised inhomogeneity in the temperature profile is rapidly removed, well before substantial changes to the flow profile occur. A side-effect is that the temperature gradient profiles are less well controlled, so that the simulations with larger diffusivities tend to have lower local temperature gradients.

For pure toroidal flows (Fig. 7(b)), the transport does almost completely stabilise for sufficiently strong positive V-flows, at about 1.5 times the level needed for negative V-flows. Another important feature is that the dynamics of $E \times B$ and parallel flows are qualitatively

quite different. The $E \times B$ flow evolution is similar to that in the pure poloidal flow cases, so that for large positive V-flow, $\omega_{E \times B}$ decreases to the saturation level, but otherwise remains roughly constant. The toroidal flow evolution, on the other hand, looks like a simple diffusion process dependent on the turbulence level, with the originally V-shaped parallel flow profile itself evolving to a smooth hump in cases where there is a substantial turbulence level (Figure 4(b) is typical).

It would be difficult to explain these global flow dynamics using a 1D transport equation, where poloidal and toroidal flow dynamics are determined via momentum fluxes dependent on the local gradients. For pure poloidal flows, there is little global flow reorganisation in the system with homogeneous shear flows. If we used the homogeneous shear simulations as a basis for a model of flow dynamics, we would also expect to see little poloidal flow evolution in the simulations with V-shaped flows, but we do see a strong flow reorganisation. In both pure toroidal and pure poloidal flow simulations, the effective (toroidal or poloidal) momentum diffusivity is strongly dependent on the sign of the flow profile, which is surprising, because flux-tube models of up-down symmetric equilibria are symmetric with respect to the sign of the shearing rate.

IV. DISCUSSION AND CONCLUSIONS

We have modelled the effects of two different forms of flow profiles on turbulence levels, and examined the time evolution of the flow profile. For homogeneous flow shear profiles, both toroidal and poloidal flow can competely suppress turbulence for some parameter choices, well above the Dimits shift region. Little $E \times B$ flow profile evolution is seen on the timescale of the simulation for homogeneous flows. On the other hand, for the non-homogeneous flow profiles, the $E \times B$ component of positive V-shaped flow profiles can rapidly decay to a saturated state.

The results help to explain why small-scale zonal flows and large scale homogeneous shear flows have different impacts on turbulence. Inhomogeneities, and, in particular, zonal flow boundaries, play a crucial role and can modify the turbulent dynamics over a substantial region. For the V shaped profiles, dynamics over a simulation domain ~ 150 gyroradii wide is critically modified when a flow shear boundary is introduced. The zone boundaries appear to control poloidal flow reorganisation in these systems, and induce the saturation in $E \times B$

shear flow level seen in typical ITG simulations. The poloidal flow does not saturate in simulations with homogeneous imposed fields, where no zone boundaries are present.

In addition, the thermal and toroidal momentum fluxes depend not only on the magnitude of the local $E \times B$ shearing rate, but on the overall flow profile over a wide region. The presence of strong nonlocal effects is correlated with the presence of bursts which can traverse a wide radial extent in strongly sheared plasmas.

This allows some insight into the effects of more general flow profiles which would be relevant to experiments, which are not generally homogeneous. For example, flow profiles associated with transport barriers have relatively short wavelength features. Models of transport barriers using homogeneous shear flows might predict stabilisation for strong enough shear, but the saturation effect shown here may limit the shearing rate and prevent turbulence supression.

Acknowledgements

[1] S. Jolliet, A. Bottino, P. Angelino, R. Hatzky, T. Tran, B. McMillan, O. Sauter, K. Appert, Y. Idomura, and L. Villard, Computer Physics Communications **177**, 409 (2007).

[2] A. G. Peeters, D. Strintzi, Y. Camenen, C. Angioni, F. J. Casson, W. A. Hornsby, and A. P. Snodin, Physics of Plasmas **16**, 042310 (2009).

[3] P. Angelino, A. Bottino, R. Hatzky, S. Jolliet, O. Sauter, T. Tran, and L. Villard, Physics of Plasmas **13**, 052304 (2006).

[4] J. Kinsey, R. Waltz, and J. Candy, Physics of Plasmas **12**, 062302 (2005).

[5] B. McMillan, S. Jolliet, T. Tran, A. Bottino, A. P., and L. Villard, Physics of Plasmas **15**, 052308 (2008).

[6] R. Waltz, R. Dewar, and X. Garbet, Physics of Plasmas **5**, 1784 (1998).

[7] F. J. Casson, A. G. Peeters, Y. Camenen, W. A. Hornsby, A. P. Snodin, D. Strintzi, and G. Szepesi, Physics of Plasmas **16**, 092303 (2009).

[8] B. McMillan, S. Jolliet, T. Tran, A. Bottino, A. P., and L. Villard, Physics of Plasmas **16**, 022310 (2009).

[9] P. Diamond and T. Hahm, Physics of Plasmas **2**, 3640 (1995).

[10] M. N. Rosenbluth and F. L. Hinton, Phys. Rev. Lett. **80**, 724 (1998).

[11] A. M. Dimits, G. Bateman, M. A. Beer, B. I. Cohen, W. Dorland, G. W. Hammett, C. Kim, J. E. Kinsey, M. Kotschenreuther, A. H. Kritz, et al., Physics of Plasmas **7**, 969 (2000).

[12] B. N. Rogers, W. Dorland, and M. Kotschenreuther, Phys. Rev. Lett. **85**, 5336 (2000).

[13] A. Dimits, B. Cohen, W. Nevins, and D. Shumaker, Nuclear Fusion **41**, 1725 (2001).

[14] Y. Idomura, H. Urano, N. Aiba, and S. Tokuda, Nuclear Fusion **49**, 065029 (2009).